Giant second-harmonic generation efficiency and ideal phase matching with a double ε-near-zero cross-slit metamaterial

Christos Argyropoulos,[1] Giuseppe D'Aguanno,[2] and Andrea Alù[1,*]

[1]*Deptartment of Electrical & Computer Engineering, The University of Texas at Austin, Austin, Texas 78712, USA*

[2]*AEgis Tech., Nanogenesis Division, 410 Jan Davis Dr., Huntsville, Alabama 35806, USA*

(Received 3 March 2014; revised manuscript received 16 May 2014; published 3 June 2014)

Efficient second-harmonic generation may be induced based on the anomalous tunneling properties of double zero-permittivity narrow cross-slit nonlinear channels. Ideal phase matching conditions, large coherence length, combined with uniform field enhancement entail the ideal conditions to achieve giant second-harmonic conversion efficiencies for backward and forward signals. It is shown that these conditions are particularly well suited to enhance nonlinear effects over a wide range of frequencies, leading to efficient electromagnetic wave mixers and parametric amplifiers.

DOI: 10.1103/PhysRevB.89.235401 PACS number(s): 41.20.Jb, 42.65.Wi, 42.70.Nq, 78.67.Pt

I. INTRODUCTION

Since the first pioneering experiments on second-harmonic generation (SHG) [1], the quest for high conversion efficiencies in nonlinear second-order optical processes has been one of the most active research areas in optical physics [2]. In general, two conditions need to be satisfied to obtain strong nonlinear effects: large nonlinear material response and phase matched interaction with electromagnetic waves. The former can be achieved by either employing highly nonlinear crystals [3] or by increasing the local density of states (LDOS) with resonant micro-cavities [4], photonic crystals [5–7] and plasmonic structures [8,9]. Phase matching is as important as a strong nonlinear material response, since efficient generation requires that all portions of the nonlinear effect interfere constructively. Phase matching schemes typically involve the use of birefringent crystals [10,11], Bragg gratings [12], or quasiphase matching (QPM) schemes [13]. The recent advent of metamaterials [14,15] has nonetheless opened new and exciting venues. In particular, SHG has been demonstrated with magnetic metamaterials [16], periodically nanostructured metal films [17], metacrystals [18], noncentrosymmetric shaped metallic nanoapertures [19], electrically controlled plasmonic gratings [20], and negative-index metamaterials [21]. In these cases, strong resonant fields and associated large LDOS have been shown to significantly boost SHG processes. In addition, phase matching can be more easily achieved in negative-index metamaterials [22–24], even if limited to the reflected (not the transmitted) second-harmonic wave, acting as a "nonlinear mirror."

Here we discuss a different mechanism to achieve an ideal phase matching condition (both in forward and backward operation) for fundamental and generated frequencies, at the same time also inducing drastically enhanced LDOS and nonlinear effects, using the unique properties of a metamaterial composed of arrays of double ε-near-zero (ENZ) crossed plasmonic channels [25]. Narrow waveguides operated at the cutoff of their dominant plasmonic mode have been recently proposed to provide a quasistatic spatial response with constant phase (ideally infinite phase velocity) and largely enhanced fields, crucial features when exciting electrically-large nonlinear samples. SHG processes in zero-index transmission lines have been demonstrated at microwaves to exploit their phase-matching advantages [26]. However, this design is limited to the microwave regime, for which nonlinearities are inherently stronger, and it therefore does not focus on local nonlinearity enhancements. The use of near-zero-index fishnet metamaterials [27] has been also proposed to boost forward and backward nonlinear generation, a scheme that allows to compensate for phase mismatch at a single frequency, but would not work to phase match fundamental and generated frequencies, as in second-harmonic processes, and again it does not allow substantial nonlinearity enhancement. Multiresonant plasma films [28] have been theoretically proposed in this context, but they are highly mismatched to free space other than at the polaritonic angle, and their field enhancement is generally limited. In the following, we discuss a different concept to produce largely enhanced LDOS at fundamental and second-harmonic frequencies, at the same time supporting ideal phase matching conditions, based on the proper engineering of arrays of narrow, crossed plasmonic channels supporting a strong double ENZ response for the fundamental and second-harmonic frequencies. In addition, the resulting metamaterial is impedance matched to free space for all incidence angles, and support ideal phase matching features, extreme coherence lengths, and uniformly, large field enhancements across the channels, leading to a new paradigm to realize uniquely large conversion efficiencies.

II. DOUBLE ε-NEAR-ZERO CROSS-SLIT METAMATERIAL

Consider a periodic array of cross-slit channels carved in a perfect electric conductor (PEC) screen, as shown in the inset of Fig. 1(d), each essentially forming two orthogonal rectangular waveguides supporting orthogonally polarized transverse-electric (TE) electromagnetic modes. We can tune the widths of the two arms such that the cutoff frequencies coincide with the fundamental and second-harmonic frequencies of interest. Following our work on metallic screens perforated by periodic arrays of rectangular narrow slits [29], we expect that the proposed array of crossed apertures operates as a

*alu@mail.utexas.edu

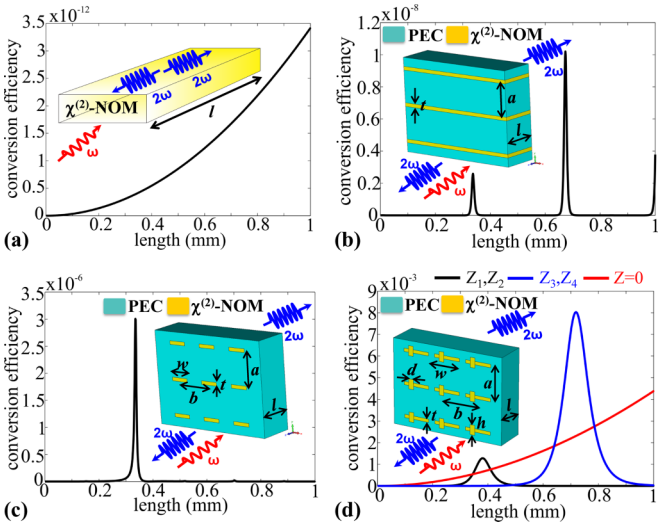

FIG. 1. (Color online) SH conversion efficiency vs slab thickness for (a) a slab made by a quadratic nonlinear dielectric (shown in the inset); (b) a parallel-plate waveguide, where the same nonlinear material is sandwiched between PEC layers (shown in the inset); (c) an array of rectangular waveguides, in which narrow rectangular apertures are loaded with the same nonlinear material (shown in the inset); (d) an array of cross-slit channels loaded with the same nonlinear dielectric (shown in the inset). Three different cases are shown in Fig. 1(d): Z_1, Z_2 (black line), Z_3, Z_4 (blue line) and no (red line) reactive impedances in the TL model of the slab interfaces. All devices are illuminated at normal incidence.

double ENZ metamaterial at the fundamental and second-harmonic frequency for the two orthogonal polarizations, each corresponding to the cutoff frequency of one of the arms, with the additional property of being impedance matched to free space for any incidence angle at both frequencies. Due to its low index, infinite phase velocity is expected inside each channel at the two frequencies, with uniformly enhanced fields, boosted by a factor proportional to the area of the periodic unit cell normalized to the waveguide aperture [29]. Notice how the axis of the vertical channel is slightly shifted off-center from the axis of the horizontal channel, to achieve maximum field enhancement inside both channels, and at the same time ensuring large modal overlap for enhanced nonlinear response.

The phase mismatch between fundamental and generated frequencies can be quantified by considering the coherence length $L_{\rm coh} = \pi/\Delta k$, where $\Delta k = (2\omega/c)\,(n_{2\omega} - n_\omega)$ and n_ω and $n_{2\omega}$ are the effective refractive indices seen by the electromagnetic wave at the fundamental and second-harmonic frequencies, respectively. In our double ENZ medium, both refractive indices are effectively $n_{2\omega} = n_\omega = 0$ and ideal phase matching is automatically achieved, with an infinite coherence length if losses are negligible. Interestingly, the proposed design can be implemented over a broad frequency range, from microwaves to the optical regime. For simplicity and to be able to operate in a regime where conduction losses are negligible, we focus our design in the low-terahertz frequency range. Note that very interesting nonlinear applications exist in this frequency range. At higher frequencies, the PEC walls considered here can be substituted by plasmonic metals [29], and similar effects may be obtained with slightly deteriorated SHG performance due to the higher conductive losses.

In order to highlight the potential of the proposed paradigm for giant conversion efficiency using double ENZ metamaterials, Fig. 1 compares four geometries of interest, as sketched in the four insets: a simple phase-matched slab of quadratic material [Fig. 1(a)]; a one-dimensional array of parallel-plate channels filled with the same material [Fig. 1(b)]; a two-dimensional array of rectangular waveguides [Fig. 1(c)]; the cross-slit array described above [Fig. 1(d)], again filled with the same nonlinear material. First, we investigate the SHG conversion efficiency of the simplest geometry, i.e., a slab with linear permittivity $\varepsilon_L = 2.25$ and second-order susceptibility $\chi^{(2)} = 20\ pm/V$ [2], schematically shown in the inset of Fig. 1(a). The medium is assumed to be phase matched at the fundamental $f_{\rm FF} = 297.4$ GHz and second-harmonic $f_{\rm SH} = 594.8$ GHz frequencies with linear refractive indices $n_{2\omega} = n_\omega = 1.5$ and it is illuminated with low pump intensity $I_{\rm in} = 258.3\ {\rm W/cm^2}$ at the fundamental frequency. Due to ideal phase-matching, the SHG conversion efficiency is given by the textbook formula [30] $\eta = \frac{2\mu_0}{n_\omega^2 n_{2\omega} c}(\frac{\chi^{(2)}}{2}\omega l)^2 I_{\rm in}$, where l is the slab thickness and c the speed of light. The conversion efficiency grows as l^2, consistent with Fig. 1(a).

Next, we investigate the parallel-plate array geometry, composed of the same nonlinear material sandwiched between metallic layers, as shown in the inset of Fig. 1(b). In this geometry, originally analyzed for third-order nonlinear effects in Ref. [31], Fabry-Pérot (FP) transmission resonances are expected for $\beta = N\pi/l$, with N being an integer, able to boost the field in the nonlinear material and therefore enhance its nonlinear response. We simulate its response using commercial software based on the finite integration method [32]. For this example, we assume dimensions $a = 440\,\mu$m, $t = 44\,\mu$m, and thickness $l = 336\,\mu$m. A dielectric material with permittivity $\varepsilon_L = 2.25$ is loaded inside the channels. The calculated transmission is plotted in Fig. 2. Two Fabry-Pérot (FP) transmission resonances are obtained at 297 and 594 GHz. Hence the first FP resonance is the fundamental frequency (FF) mode and the second is the second-harmonic (SH) mode when second-order nonlinearities are introduced inside the waveguide's channel.

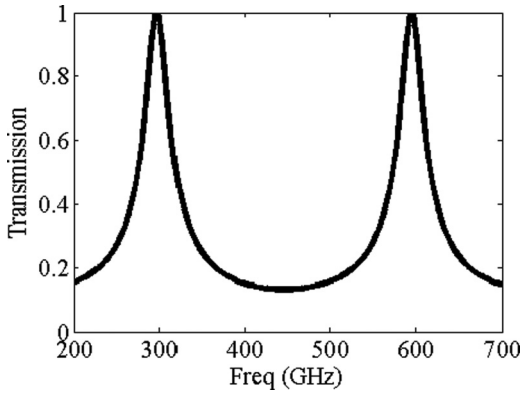

FIG. 2. Transmission vs frequency of the parallel-plate waveguide shown in the inset of Fig. 1(b).

The calculated conversion efficiency versus thickness, calculated for $a = 440\,\mu$m, $t = 44\,\mu$m, and shown in Fig. 1(b), shows negligible conversion except at the FP resonant peaks, at which the expected enhancement is around $a/t \simeq 10$. We note here that, due to the ideality of the metal, FP resonances align at the fundamental and second-harmonic frequency. The total (forward plus backward) SHG conversion efficiency can be calculated in terms of overlap integrals [21]:

$$\eta = \frac{\omega_{\mathrm{FF}}^2}{2\varepsilon_0\varepsilon_L c_0^3}\left(\left|\int_0^l \chi^{(2)}(E_\omega^{(+)})^2 E_{2\omega}^{(-)} dz\right|^2 + \left|\int_0^l \chi^{(2)}(E_\omega^{(+)})^2 E_{2\omega}^{(+)} dz\right|^2\right) I_{\mathrm{in}}, \quad (1)$$

where $\omega_{\mathrm{FF}} = 2\pi f_{\mathrm{FF}}$, $E_\omega^{(+)}$ is the right-to-left (forward) field distribution inside each waveguide at the fundamental frequency and $E_{2\omega}^{(+)}$, $E_{2\omega}^{(-)}$ are the right-to-left (forward) and left-to-right (backward) field distributions at the second-harmonic frequency. In our calculations, we used full-wave simulations [32] to evaluate the reactive fields at the entrance and exit of the slits, in order to properly model the interfaces with lumped elements, and then implemented a transmission-line analytical model to efficiently evaluate the effect of varying the slab thickness. For sample thicknesses, we validated the accuracy of our model with full-wave simulations.

Equation (1) implies that large efficiencies may be achieved if the fields are enhanced at both fundamental and generated frequencies, as it occurs at the FP resonances. Indeed, at the two FP peaks, four orders of magnitude enhancement are observed compared to the bulk quadratic material of Fig. 1(a). We note that the first SHG conversion peak, found for $l = 336\,\mu$m has a half-power bandwidth (HPBW) of $10.4\,\mu$m. Similar SHG conversion efficiencies follow for longer slits, when other FP resonances overlap at fundamental and second-harmonic frequencies. The SHG peak values grow approximately as the square of the channel's length.

One of the drawbacks of this resonant design is that it requires the careful overlap of two different FP resonances in the same structure, which may not be easy in the realistic scenarios in which the metal has dispersion, as we have only one parameter to effectively control the resonances, i.e., the slab thickness. In addition, the channel length is not exploited at its best, since the FP modes in the slits are characterized by standing wave distributions with different phases. In order to overcome these issues, we consider rectangular channels, which we have shown in the past to support an anomalous tunneling effect at the cutoff frequency of their dominant mode, due to ENZ tunneling with infinite phase velocity [29]. In this regime, uniformly enhanced field distributions are expected all along the channel, able to use more efficiently the slab thickness. This geometry is shown in Fig. 1(c), which is consistent with the silver grating proposed in Ref. [29] to boost third-order nonlinearities. The dimensions of the structure are tuned so that ENZ tunneling is supported at the fundamental frequency, while the second-harmonic coincides with the second FP resonance. These are quite easy to control and align, even in the case of realistic metal dispersion, since the width b of the channels controls the cutoff (ENZ operation), while the thickness l controls the FP resonances. The grating shown in the inset of Fig. 1(c) was simulated using [32] and its transmission is plotted in Fig. 3. It has dimensions: $a = 440\,\mu$m, $b = 440\,\mu$m, $t = 44\,\mu$m, and $w = 334\,\mu$m, and thickness $l = 335\,\mu$m. Again, dielectric material with permittivity $\varepsilon_L = 2.25$ is loaded inside the channels of the grating. Now, an epsilon-near-zero (ENZ) resonance is obtained at 311 GHz followed by two sharp FP resonances. The second FP resonance is obtained at 622 GHz, exactly at double frequency value compared to the ENZ resonance. As a result, the ENZ resonance is the FF mode and the second FP resonance is the SH mode when second-order nonlinearities are introduced inside the waveguide's channel. The fields at these two resonances are used to compute Eq. (1) and

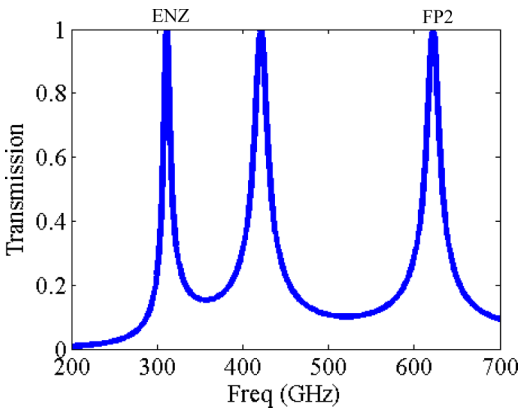

FIG. 3. (Color online) Transmission vs frequency of an array of rectangular waveguides shown in the inset of Fig. 1(c).

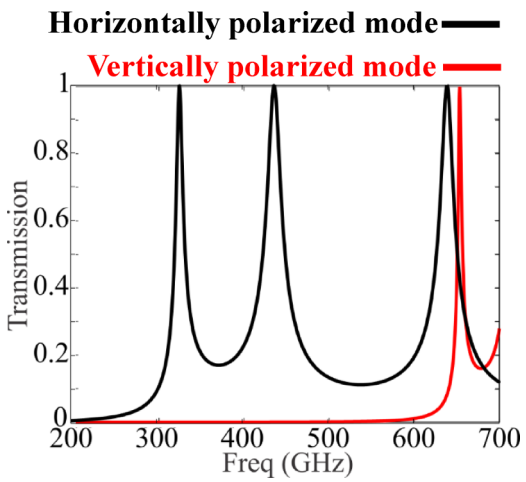

FIG. 4. (Color online) Transmission of horizontally and vertically polarized modes impinging on the cross-slit grating shown in the inset of Fig. 1(d). The ENZ transmission corresponds to the first transmission peak, followed by FP resonances.

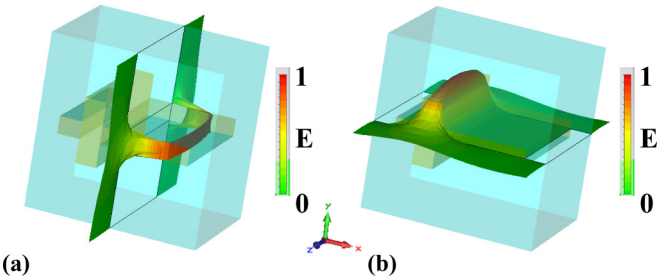

FIG. 5. (Color online) 3D normalized electric field distributions for (a) horizontal and (b) vertical polarized radiation in the cross-slit waveguide shown in the inset of Fig. 1(d). The cross-slit channels are shown with light yellow shaded regions.

Fig. 1(c) shows the calculated efficiency. The enhancement in SHG conversion efficiency is six orders of magnitude larger compared to the bulk quadratic material and two orders of magnitude larger than the slit geometry with same thickness. The HPBW $= 8.1\,\mu$m is still quite narrow.

Finally, we analyze the proposed cross-slit array shown in the inset of Fig. 1(d). The optimized geometry has $a = 440\,\mu$m, $b = 440\,\mu$m, $t = 44\,\mu$m, $w = 334\,\mu$m, $d = 53\,\mu$m, $h = 165\,\mu$m, and $l = 380\,\mu$m. This structure can sustain two distinct and independently controllable cutoff frequencies for orthogonally polarized TE modes, being able to fully exploit the ENZ anomalous tunneling features at both fundamental and second-harmonic frequencies. This is seen in more detail in Fig. 4, in which we show the transmission spectra for the two polarizations [32]. The three-dimensional (3D) electric field distributions of the horizontal and vertical polarized ENZ modes supported by the cross-slit grating are shown in Fig. 5. The results are obtained using numerical simulations [32]. The fields have uniform phase and they are enhanced across the channel of the waveguide at both ENZ modes. These are ideal conditions to obtain giant SHG conversion efficiency. The cross-slits support quasi-TE modes with a dominant electric field component similar to the single rectangular aperture. The cutoff frequency for vertical polarization is $f^{\mathrm{V}}_{\mathrm{ENZ}} = 326\,$GHz, slightly larger compared to the one obtained in Fig. 1(c) for the same transverse width, due to the detuning introduced by mode coupling in the cross-slit channels. The additional slit, rotated by ninety degrees, supports a similar response for horizontal polarization. Its cutoff frequency is controlled by d, and it is tuned here at the second-harmonic frequency $f^{\mathrm{H}}_{\mathrm{ENZ}} = 652\,$GHz.

III. GIANT SHG GENERATION EFFICIENCY

We assume now that the quadratic material filling the cross-slit waveguide has an anisotropic nonlinear tensor $\chi^{(2)}_{yyx} = 20\,pm/V$. Note that nonlinear crystals with such anisotropic nonlinear tensor are quite common, and widely used in nonlinear processes [2,33]. In order to compute the SHG conversion efficiency, we again use Eq. (1), using our analytical TL model. Inductive loads with impedances $Z_1 = j116.7\,\Omega$, $Z_2 = j58.5\,\Omega$ are considered to properly take into account the reactive fields at the two interfaces for vertical and horizontal polarizations, respectively, as extracted from full-wave simulations. The proposed geometry is able to convert the large enhancement at the fundamental frequency in the longer arm of the cross-slit into second-harmonic nonlinear horizontal polarization, coupling into the ENZ mode in the shorter arm of each aperture. In this way, we achieve both ideal phase matching, due to the double ENZ condition, and large enhancement of the quadratic nonlinearity, due to the uniform distribution at both FF and SH fields along the channels. This leads to very large SHG conversion efficiencies, shown by the black line in Fig. 1(d), which also are characterized by a much broader HPBW $= 65.5\,\mu$m, compared to the previous examples. This result introduces a remarkable paradigm for large generation efficiency, which may be achieved without requiring increased Q factors and sharper resonances, but are instead based on ideal phase matching at the double ENZ tunneling condition. The SHG peak is found for channels with length $l = 380\,\mu$m, where both fundamental and second-harmonic modes exhibit the ENZ response.

In order to further highlight the different physics arising in this double ENZ metamaterial slab, we show that for different inductive load values ($Z_3 = j114.8\,\Omega$, $Z_4 = j57.9\,\Omega$), which may be achieved by coating the entrance and exit interfaces,

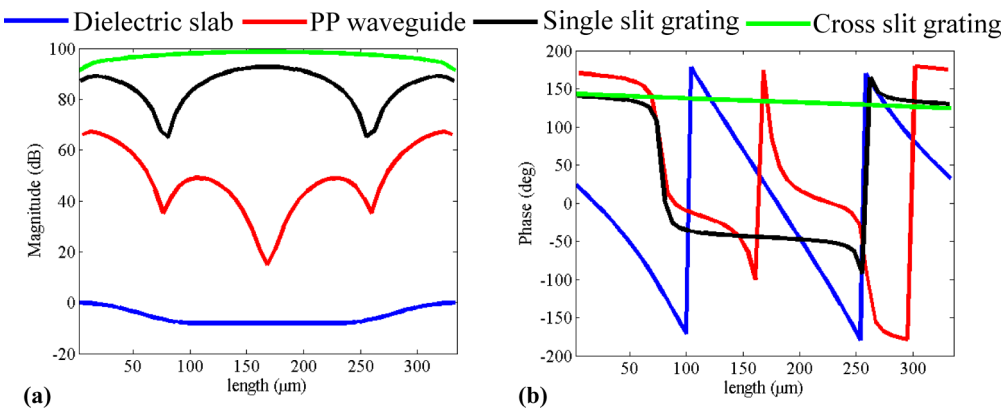

FIG. 6. (Color online) (a) Magnitude (dB) and (b) phase (degrees) of the quantity $E^2_{\omega}E_{2\omega}$, where E_{ω} and $E_{2\omega}$ are the field enhancement inside the channels of all the structures under study. In this case, the waveguide channels are assumed to have equal length $l = 336\,\mu$m. Large and homogeneous magnitude combined with constant phase along the channel of the cross slit double ENZ grating leads to very large values in the SHG efficiency, which is calculated by Eq. (1).

will lead to shifted and even larger SHG conversion efficiencies, shown with the blue line in Fig. 1(d), and an even broader HPBW = 99.5 μm. This is due to the fact that the SHG peak is essentially dominated by the resonant tunneling supported by the reactive fields at the entrance and exit interfaces. If we were able to neglect the stored reactive fields at the channel's interfaces and assume zero shunt admittance at the two interfaces, we would obtain a quadratic dispersion for the SHG conversion efficiency, as the red line in Fig. 1(d), similar to the bulk phase-matched case in Fig. 1(a). In this case, the nonresonant SHG conversion efficiency is nine orders of magnitude larger compared to the performance of Fig. 1(a), yet supporting an extremely broad response, automatically phase matched for any length of the slab. These results may also be extended to higher frequencies, but expecting lower SHG conversion efficiency and a limited coherence length, due to the larger conductivity losses in metals.

To provide further insight into this phenomenon, we show in Figs. 6(a) and 6(b) the magnitude and phase of the quantity $E_{\omega}^{2}E_{2\omega}$, i.e., the overlap integrand in Eq. (1), for excitation from one side of the grating. This quantity is computed for each of the four geometries of Fig. 1, and plotted versus the length of the structure for same length $l = 336\mu$m for fair comparison. The figure beautifully summarizes the operation of the proposed metamaterial. While the simple dielectric slab has no field enhancement, the parallel-plate slits provide some field enhancement, but characterized by a standing-wave pattern and a fast phase variation. When integrated over the channel length, the large field enhancement is actually not efficiently exploited. The rectangular slits support a stronger field enhancement and slower phase variation, along the channel length the integrand has opposite phase contributions. The cross-slit grating supports larger field enhancement, uniformly distributed along each channel, and a flat phase response, ideal to maximize the integrals in Eq. (1), consistent with the giant enhancements predicted in Fig. 1(d).

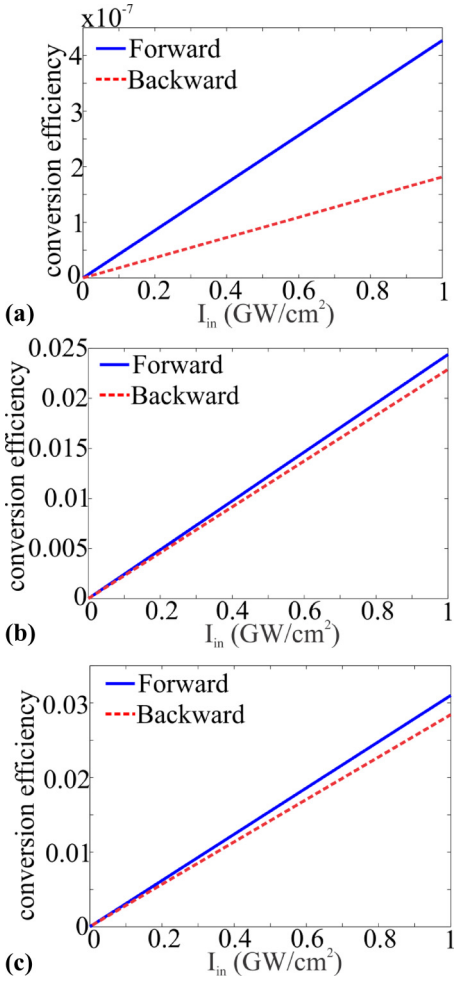

FIG. 7. (Color online) Forward (blue solid) and backward (red dashed) SH conversion efficiencies changing with the input intensity (I_{in}) for (a) a nonlinear dielectric slab with parameters $n = 2.5$, $\chi^{(2)} = 20$ pm/V, and length $l = 336\,\mu$m; (b) the nonlinear single-slit grating with same parameters as the one shown before in the inset of Fig. 1(c) in the paper and length $l = 335\,\mu$m; and (c) the nonlinear cross-slit grating with same parameters as the one shown before in the inset of Fig. 1(d) in the paper and length $l = 380\,\mu$m. Great enhancement in forward and backward conversion efficiencies is obtained for both gratings compared to the bare nonlinear dielectric slab.

IV. BALANCED FORWARD AND BACKWARD SH GENERATION

Next, coupled-mode theory is used [34] to further verify the enhanced SHG potentials of the proposed waveguide designs. First, forward and backward SH conversion efficiencies as a function of input intensity (I_{in}) are shown in Fig. 7(a) for a quadratic dielectric slab [similar to the inset in Fig. 1(a)] with linear refractive index $n = 2.5$, nonlinear susceptibility $\chi^{(2)} = 20pm/V$ and length $l = 336\,\mu$m. Low SHG efficiency is obtained for both forward and backward second-harmonic waves. The second-harmonic signal is stronger in the forward direction, leading to unbalanced SHG. As a next step, we compute the SHG conversion efficiencies for the single-slit grating shown in the inset of Fig. 1(c), with similar dimensions and material parameters described before. The results are shown in Fig. 7(b) and the SHG performance is largely enhanced compared to Fig. 7(a). Interestingly, in this case, the SH signals are generated almost in a perfectly balanced way in forward and backward directions, as expected in high feedback systems [21]. Finally, we compute the SHG conversion efficiencies versus the input intensity for the proposed cross-slit waveguide structure, shown in the inset of Fig. 1(d). Even higher SHG performance is obtained in Fig. 7(c), and forward and backward second-harmonic signals are generated nearly balanced. This further proves that the proposed cross-slit double ENZ slab provides an ideal nonlinear configuration towards enhancing forward and backward second-harmonic generation.

V. CONCLUSIONS

To conclude, we have proposed a novel nonlinear mechanism to achieve phase-matching combined with uniform and enhanced fields for both fundamental and second-harmonic signals. This directly leads to strong nonlinear effects and giant SHG conversion efficiencies. A cross-slit nonlinear dual ENZ slab has been designed to implement this concept. Huge SHG conversion efficiencies are predicted for both forward and

backward second-harmonic signals, even though the structure has a high degree of symmetry. We envision a plethora of nonlinear applications opened by this technology, including all-optical switching, efficient wave mixing and ultrahigh resolution near-field microscopy. It is straightforward to extend the demonstrated cross-slit design to higher frequencies, where PEC materials are substituted by noble metals (Ag, Au). The SHG performance will be slightly affected in this case, due to increased conductive losses of metals at optical frequencies, but still higher values are expected compared to conventional SHG schemes. Moreover, the proposed giant SHG mechanism is not expected to be sensitive to the incidence angle, since the ENZ response is not affected by transverse spatial dispersion. As a final remark towards the practical implementation of the proposed structure, we need to stress that the cross-slit waveguide may be embedded in quadratic nonlinear materials, which will be used as a substrate without affecting the predicted SHG operation of the device. We believe that the present work may lead one step closer to highly efficient nonlinear devices.

ACKNOWLEDGMENTS

This work has been supported by the ARO STTR project "Dynamically Tunable Metamaterials," the AFOSR YIP award No. FA9550-11-1-0009, the ONR MURI grant No. N00014-10-1-0942 and the DARPA SBIR project "Nonlinear Plasmonic Devices."

[1] P. Franken, A. Hill, C. Peters, and G. Weinreich, Phys. Rev. Lett. **7**, 118 (1961).
[2] R. W. Boyd, *Nonlinear Optics* (Academic, London, 1992).
[3] V. G. Dmitriev, G. G. Gurzadyan, and D. N. Nikogosyan, *Handbook of Nonlinear Optical Crystals* (Springer, New York, 1997).
[4] H. Cao, D. B. Hall, J. M. Torkelson, and C.-Q. Cao, Appl. Phys. Lett. **76**, 538 (2000).
[5] M. Soljacic and J. D. Joannopoulos, Nat. Mater. **3**, 211 (2004).
[6] G. D'Aguanno, M. Centini, M. Scalora, C. Sibilia, Y. Dumeige, P. Vidakovic, J. A. Levenson, M. J. Bloemer, C. M. Bowden, J. W. Haus, and M. Bertolotti, Phys. Rev. E **64**, 016609 (2001).
[7] F.-F. Ren, R. Li, C. Cheng, H.-T. Wang, J. Qiu, J. Si, and K. Hirao, Phys. Rev. B **70**, 245109 (2004).
[8] W. L. Barnes, A. Dereux, and T. W. Ebbesen, Nature (London) **424**, 824 (2003).
[9] W. Fan, S. Zhang, N.-C. Panoiu, A. Abdenour, S. Krishna, R. M. Osgood, Jr., K. J. Malloy, and S. R. J. Brueck, Nano Lett. **6**, 1027 (2006).
[10] J. A. Giordmaine, Phys. Rev. Lett. **8**, 19 (1962).
[11] P. D. Maker, R. W. Terhune, M. Nisenoff, and C. M. Savage, Phys. Rev. Lett. **8**, 21 (1962).
[12] C. L. Tang and P. P. Bey, IEEE J. Quantum Electronics **9**, 9 (1973).
[13] M. M. Fejer, G. A. Magel, D. H. Jundt, and R. L. Byer, IEEE J. Quantum Electronics **28**, 2631 (1992).
[14] J. B. Pendry, A. J. Holden, D. J. Robbins, and W. J. Stewart, IEEE Trans. Microwave Theory Tech. **47**, 2075 (1999).
[15] A. A. Zharov, I. V. Shadrivov, and Y. S. Kivshar, Phys. Rev. Lett. **91**, 037401 (2003).
[16] M. W. Klein, C. Enkrich, M. Wegener, and S. Linden, Science **313**, 502 (2006).
[17] A. Nahata, R. A. Linke, T. Ishi, and K. Ohashi, Opt. Lett. **28**, 423 (2003).
[18] D. Huang, A. Rose, E. Poutrina, S. Larouche, and D. R. Smith, Appl. Phys. Lett. **98**, 204102 (2011).
[19] P. Schön, N. Bonod, E. Devaux, J. Wenger, H. Rigneault, T. W. Ebbesen, and S. Brasselet, Opt. Lett. **35**, 4063 (2010).
[20] W. Cai, A. P. Vasudev, and M. L. Brongersma, Science **333**, 1720 (2011).
[21] N. Mattiucci, G. D'Aguanno, M. J. Bloemer, and M. Scalora, Phys. Rev. E **72**, 066612 (2005).
[22] I. V. Shadrivov, A. A. Zharov, and Y. S. Kivshar, J. Opt. Soc. Am. B **23**, 529 (2006).
[23] A. K. Popov and V. M. Shalaev, Appl. Phys. B **84**, 131 (2006).
[24] A. Rose, D. Huang, and D. R. Smith, Phys. Rev. Lett. **107**, 063902 (2011).
[25] A. Rose and D. R. Smith, Opt. Mater. Express **1**, 1232 (2011).
[26] W. R. C. Somerville, D. A. Powell, and I. V. Shadrivov, Appl. Phys. Lett. **98**, 161111 (2011).
[27] H. Suchowski, K. O'Brien, Z. J. Wong, A. Salandrino, X. Yin, and X. Zhang, Science **342**, 1223 (2013).
[28] M. A. Vincenti, D. de Ceglia, J. W. Haus, and M. Scalora, Phys. Rev. A **88**, 043812 (2013).
[29] C. Argyropoulos, P.Y. Chen, G. D'Aguanno, N. Engheta, and A. Alù, Phys. Rev. B **85**, 045129 (2012).
[30] A. Yariv and P. Yeh, *Optical Waves in Crystals* (Wiley, New York, 1984).
[31] J. A. Porto, L. Martın-Moreno, and F. J. Garcıa-Vidal, Phys. Rev. B **70**, 081402(R) (2004).
[32] CST Design Studio 2011, www.cst.com.
[33] J. A. Armstrong, N. Bloembergen, J. Ducuing, and P. S. Pershan, Phys. Rev. **127**, 1918 (1962).
[34] G. D'Aguanno, M. Centini, M. Scalora, C. Sibilia, M. Bertolotti, M. J. Bloemer, and C. M. Bowden, J. Opt. Soc. Am. B **19**, 2111 (2002).